Chemistry—Methods

Research Article
doi.org/10.1002/cmtd.202500105

Chemistry Europe
European Chemical Societies Publishing

www.chemistrymethods.org

Spectroscopic Reactor for *Operando* Investigations Made by Additive Manufacturing for High-Pressure Catalysis Applications

Mariam L. Schulte, Vera Truttmann, Lorena Baumgarten, Alexander G. Nicolai, Diego A. Montalvo Beltran, Florian J. Summ, Christoph Kiener, Erisa Saraçi, and Jan-Dierk Grunwaldt*

Knowledge-based catalyst design requires the identification of the active structure during reaction, i.e., by *operando* spectroscopy, and at different conversion levels. However, for reactions that run at elevated pressure, such as methanol, Fischer–Tropsch, or ammonia synthesis, obtaining spectroscopic data at realistic conditions remains a major challenge. In particular, standard *operando* setups often fail to replicate the high-pressure, high-conversion regimes relevant to industrial processes. This requires specially designed reactors, and here, how additive manufacturing enables the development of spectroscopic reactors for *operando* studies of catalysts under high-pressure conditions at different conversion levels up to equilibrium is reported. The reactor has two consecutive zones with independent temperature control and individual catalyst loading. An X-ray-transparent window in the latter zone allows for spatially resolved spectroscopic monitoring of the catalyst structure. A mobile setup is constructed for operation at a synchrotron source, and the functionality of the reactor is demonstrated in an *operando* X-ray absorption spectroscopy study using a $Cu/ZnO/ZrO_2$ catalyst during CO_2 hydrogenation to methanol. The dual-zone design enabled simulation of an end-of-catalyst-bed environment, including condensation, which is highly critical for industrial relevance yet difficult to realize in conventional *operando* experiments.

1. Introduction

Heterogeneous catalysts for industrially relevant reactions, e.g., methanol, Fischer–Tropsch, and ammonia synthesis, exhibit very dynamic structures that depend strongly on the present reaction conditions.[1–4] Given this structural sensitivity, monitoring of the catalyst structure during reaction –*operando*– is crucial to allow knowledge-based catalyst design for the development of more efficient and stable catalysts.[5,6] Due to the small volume of spectroscopic cells/reactors and the often-necessary dilution for spectroscopic investigations in transmission mode, *operando* spectroscopy studies often utilize only small amounts of catalysts.[7–10] This leads to conversions significantly lower than industrial levels, which makes extrapolation to the real process difficult.[11] This issue has recently been highlighted in ammonia decomposition/synthesis catalysts, where high ammonia concentrations have caused phase transformations, which could not be observed at lower levels.[12] To reconcile reaction and spectroscopic constraints, this study proposes placing a second catalyst bed composed of undiluted catalyst upstream, enabling high conversion and facilitating structural observation in the subsequent, diluted catalyst bed. The two-zone or two-reactor concept is employed in laboratory or technical plants to investigate two or multistep reactions and emulate spatially varying reaction conditions.[13,14] An alternative concept is the iso-potential *operando* reactor developed by Horn and colleagues.[10] Many industrial processes, such as methanol synthesis, are conducted under high pressure, posing significant challenges for spectroscopic analysis. X-ray absorption spectroscopy (XAS) is a powerful tool which allows to monitor the catalyst structure under the required conditions.[9,15,16]

Designing spectroscopic cells for catalytic applications is complex, as it requires meeting the demands of both the spectroscopic technique and the catalytic process.[6,15] For the design of XAS cells, the window materials need to be X-ray permeable. Several materials can be used such as quartz, diamond, glassy carbon, polyimide, and beryllium (Be).[8,17] The *in situ* boron

M. L. Schulte, V. Truttmann, L. Baumgarten, E. Saraçi, J.-D. Grunwaldt
Institute for Chemical Technology and Polymer Chemistry
Karlsruhe Institute of Technology
Engesserstr. 20, 76131 Karlsruhe, Germany
E-mail: grunwaldt@kit.edu

M. L. Schulte, V. Truttmann, L. Baumgarten, E. Saraçi, J.-D. Grunwaldt
Institute of Catalysis Research and Technology
Karlsruhe Institute of Technology
Hermann-von-Helmholtz-Platz 1, 76344 Eggenstein-Leopoldshafen, Germany

A. G. Nicolai, D. A. Montalvo Beltran, F. J. Summ, C. Kiener
Advanced Manufacturing & Circularity
Research & Predevelopment, Foundational Technologies
Siemens AG
Otto-Hahn-Ring 6, 81739 Munich, Germany

Supporting information for this article is available on the WWW under https://doi.org/10.1002/cmtd.202500105

nitride cell by Lytle et al.,[18] which can be used with pressures up to 100 bar, is the basis for many modern spectroscopic cells.[19] Although this design is sufficient for a range of applications, one drawback for use in catalysis is the relatively large cell volume which can lead to internal and external mass transport limitations.[20] The development of a plug–flow type reactor using quartz capillaries was a strong improvement to be closer to laboratory fixed–bed reactors and is often applied to study methanol synthesis up to 20 bar.[20–28] However, these pressures are still far below the 50–100 bar used in industry. By using fused-silica capillaries, higher pressures can be achieved, as shown by Martin et al.,[29] in an *operando* XRD study up to 50 bar, and by Bansode et al.[30] in an *operando* XAS study up to 200 bar. The sample amount, often diluted for transmission experiments, is limited in capillaries to only a few milligrams, which leads to low conversion levels. Beside the use of capillaries, different high-pressure cells were developed and applied. One approach is the use of Be tube reactors, as shown by Bare et al.[31] and Divins et al.[32] for experiments up to 40 bar. Be similar to Al has a high stability, can withstand temperatures up to 1000 °C and high pressures (>1000 bar), and is X-ray permeable. It was used as window material for several spectroscopic cells for CO_2 hydrogenation experiments up to 50 bar.[19,33–35] With the development of these cells, the conditions that could be reached got closer to the real-world scenarios, however, the gas conversion levels are still often way below equilibrium conditions. The cell reported here directly addresses this limitation through the implementation of a two-zone design concept. Currently, no *operando* XAS reactor design simultaneously enables high conversion, operation under industrially relevant pressures, spatially resolved measurements, and flexible thermal control—capabilities that are essential for investigating a variety of effects on the catalyst structure. Integrating such diverse functionalities into a single component presents significant engineering challenges and is time-intensive when relying on conventional manufacturing techniques. Moreover, geometric constraints inherent to traditional fabrication methods limit design flexibility.

These limitations can be effectively addressed through additive manufacturing (AM), which offers enhanced design freedom and the potential for rapid prototyping of complex reactor geometries. AM, also known as "3D printing" or "rapid prototyping", has been strongly emerging in recent years and is, through its versatility, being employed for a wide range of applications including catalysis.[36] AM shows many advantages: sophisticated geometries, fast production, manifold selection of materials, and smart design, which can lead to enhanced mass and heat exchange, especially when speaking of microreactors.[37] Catalytic reactors fabricated using AM are often polymer–based and used for organic reactions, electro– and photocatalysis, since those processes do not require high temperature and pressure.[38] The technique can further be used for designing spectroscopic cells as shown for photocatalysis by development of an *operando* XAS cell on polymer basis.[39] For emission control, which requires high-temperature, AM can be used to fabricate and improve ceramic monolith structures on which the catalyst is then coated.[40,41] The use of metal-based AM enables even more versatile applications in chemical engineering that are highlighted in a recent article.[42] Especially the laser-based powder bed fusion technology, where each layer is punctually welded/melted by a laser, is highly promising and can be used for a variety of materials: 1) polymers, 2) metals and composites such as steel, Ni- or Cu-alloys and a growing market of new alloys, and 3) ceramics.[36] It further allows to fabricate complex structures, such as internal cooling channels which are not accessible through conventional manufacturing. However, limitations of the technique also exist, which are mainly the 1) required support structures depending on the desired geometry and the 2) high surface roughness. The removal of structures and polishing surfaces requires additional post-processing, which can be expensive and time consuming.[36] Nevertheless, the design benefits of AM technology are being exploited in several areas of chemical engineering, namely the design of efficient heat exchangers including condensers with improved functionality through thin channels and walls for improved heat exchange, or the use of multimaterial printer as one example.[43–46]

Furthermore, open cell structures can be fabricated with AM, which through their capillary effect can enhance the removal of liquids in condensation reactor concepts.[47] This strategy can in some cases be used to shift the equilibrium to the product side to achieve higher yields, which is a promising concept for the CO_2-based methanol synthesis, and several patents for condensation reactor/concepts by Siemens AG were published.[48–52] One challenge is that at elevated pressures (above ≈90 bar), liquid product condensation can already occur at ≈180 °C which is close to the applied reaction temperature range (200–250 °C) and may also lead to condensation in the catalyst bed. This is critical since high pressure and liquids create hydrothermal conditions that might severely damage the catalyst structure.[53] Investigations of the catalyst structure under these conditions are thus especially crucial. By understanding the deactivation route, possible reactivation treatments and optimal reaction operating parameters can be elucidated.

In this work, we present the development of a spectroscopic reactor, realizable by AM, with two zones with individual temperature control and large X-ray transparent windows enabling spatially-resolved measurements at pressures up to 90 bar. The reactor allows performing *operando* XAS investigations for industrially relevant reactions, and we investigated as an example CO_2 hydrogenation to methanol using a Cu/ZnO/ZrO_2 catalyst. Its dual catalyst bed configuration enables investigations under conditions out of the ordinary, naming enforced condensation as one example. For the use at synchrotrons, a dedicated experimental mobile setup was constructed. AM made it possible to integrate several functions such as two temperature zones, thermocouple positions close to the catalyst bed, and channels for heating and cooling medium. This shows the versatility of methods which can be further utilized for the design of spectroscopic cells.

2. Results and Discussion

2.1. Design of the Additively Manufactured Spectroscopic Reactor

The aim was to design a spectroscopic cell for *operando* XAS investigations which allows investigations of the catalyst structure at stress test conditions, e.g., high pressure, close to equilibrium conditions, with sufficient catalyst amount to produce significant product amounts and during condensation of possible liquid products. As discussed above, AM is a versatile technology and strongly emerging in the last years.[54] Through its multifunctionality, AM can be utilized to design a spectroscopic reactor with the demanding requirements stated above. The first step of the reactor development was to identify boundary conditions and requirements for the use as spectroscopic reactor, from a catalysis, spectroscopy, and safety viewpoint (**Table 1**).

After identifying the requirements for the catalytic process and spectroscopy, the feasibility and limitations of AM were reviewed. While AM allows for the realization of unique geometries and designs tailored to specific needs, there are notable limitations: 1) Overhangs of less than 45° require supporting structures from beneath. Upon removal, these structures can leave a rough intersection surface, potentially compromising the functionality of components such as seals. 2) Due to the higher surface roughness of AM parts compared to traditional milling, additional post-processing steps are necessary to achieve a smooth surface. 3) Significant material gradients can lead to warping of the surface, which in turn can destabilize the pressure resistance of the application.

The final reactor used for *operando* XAS experiments with its specific features is visualized in **Figure 1**. A key feature of the reactor is the two consecutive catalyst beds with independent temperature control. The first catalyst bed (referred to as "upper part") can be filled with large amounts of undiluted catalyst to achieve high CO_2 conversion and MeOH/water yields (Figure 1a). By the top to bottom flow, the reaction mixture then reaches the second catalyst bed (referred to as "window zone"), which is radiated with X–rays (Figure 1a). The aim of this concept is to mimic the end of a fixed bed reactor and study the effect of high product concentration on the catalyst structure. By keeping the reaction temperature in the upper part stable and decreasing the temperature in the window zone, the catalyst degradation during reaction can be further investigated by inducing condensation inside the catalyst bed. A photograph of the final prototype is shown in Figure 1b. The overall dimensions of the reactor are ≈19 cm in length and a width of ≈15 cm (Figure 1c). The upper part for the first catalyst bed has a volume of ≈7 mL and can be filled with up to 10 g of undiluted catalyst. The feed gas enters the catalyst bed from the top of the reactor. The window is vertically divided by on open cell structure, which is manufactured in the same AM process as the rest of the reactor. The connection between upper part and window zone is filled with this porous material. The porous filter enables gas and liquid to pass while holding back the catalyst (sieve fraction 100–200 μm) and the used diluent (silicon carbide (SiC), 210 μm), which stay in the upper part. The quadratic window frame is 10 by 10 mm, its depth is 1.5 mm, and the void volume results to ≈0.07 mL. The diluted catalyst (sieve fraction 100–200 μm) in the window part is fixed by porous structures, also made by AM (Figure 1c). For sealing of the window zone, a stack of additively manufactured plates, graphite discs (Ø = 29 mm, thickness, 1 mm), and X–ray transparent beryllium (Be) discs (Ø = 29 mm, thickness 1.5 mm) are used on each side, as illustrated in Figure 1a. Note that Be needs to be handled with care due to safety, especially, if oxidized. The stack was secured in place with six screws and nuts. Due to the roughness (Ra ≈ 130 μm) of the AM surface, the sealing graphite discs require a minimal thickness of 300 μm, as the high pressure from the tightening fixture compresses the material. For precautionary measures, the thickness in this study was increased to 1 mm. Both local surface roughness and global surface warpage reduce the constant pressure between the graphite and the reactor. Our solution is to build a circular rise of 0.2 mm around the window

Table 1. Requirements considered for the design of the spectroscopic cell with AM.

Aspects	Requirements
Catalysis	Condensation zone: The reactor needs a zone where a temperature gradient can be induced, to study the effects of condensation on the catalyst structure. For this process, temperature control and monitoring are essential. Therefore, thermocouples should be inserted at several positions and several heating, and cooling sources are needed.
	Reaction: To achieve high conversion and sufficient MeOH yield, the reaction should be operated at pressures up to 150 bar. The connection between X-ray window zone and the reactor, and from the AM parts to the rest of the setup needs pressure tight sealing.
	Catalyst handling: Due to the thickness requirement for transmission experiments (max. thickness of 1.5 mm), only a small amount of catalyst can be used in the X-ray window area. To achieve condensation, sufficient and realistic amounts of MeOH and water need to be formed during the reaction. Therefore, a more concentrated catalyst sample has to be placed above the window zone. Furthermore, the filling and removing process of the catalyst powder as well as its fixation needs to be considered in the design.
Spectroscopy	X-ray window zone: In order to investigate the structure of the catalyst, a window area with an X-ray transparent material, e.g., Be needs to be present. Furthermore, the investigated catalyst bed should not be thicker than 1.5 mm and has to be diluted to allow XAS experiments in transmission mode.
Safety	Materials: Materials should be suitable for the used gases (H_2 and CO_2) as well as the formed products (CO, MeOH, H_2O) and need to withstand the used pressure (150 bar) and temperature (350 °C). Information on the compatibility is shown in Supporting Information, Section 1. All hazards and potential risks need to be identified and safety measures installed for safe operation. Use extra caution when handling toxic substances like Be and CO. If they can be substituted, less toxic materials/gases should be used.

Research Article
doi.org/10.1002/cmtd.202500105
Chemistry Europe
European Chemical Societies Publishing

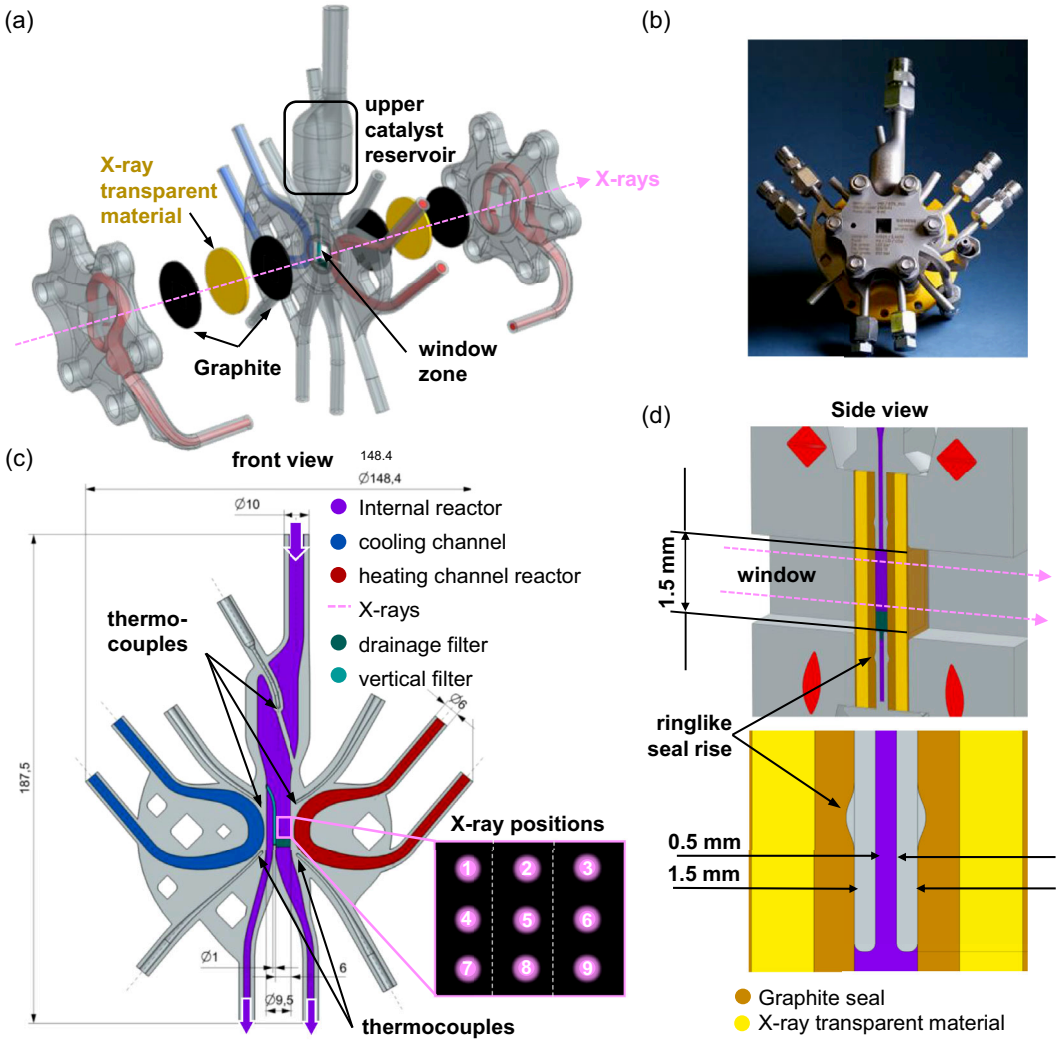

Figure 1. a) Schematic of the sealing concept of the reactor with X-ray transparent windows with 1.5 mm thickness, 1 mm thick graphite discs and plates with heating channels, marked "upper catalyst reservoir" and "window zone". b) Photograph of final spectroscopic reactor prototype. c) Front view technical drawing of the reactor, heating (marked red) and cooling (marked blue) channels inside the reactor, further inset on the 3 × 3 matrix that was scanned with X-rays during the experiment. d) Side view in technical drawing of the sealing concept.

to minimize the sealing contact area and thus increase the sealing pressure (Figure 1d).

To enable studies at different temperature conditions, the temperature of both catalyst beds can be independently controlled. For the upper part, a heating sleeve is used. Note the maximum operational temperature of the device, in this case 450 °C. To ensure the desired temperature is actually reached in the catalyst bed, a thermocouple is placed inside a channel in the middle of the upper part (Figure S2, Supporting Information). A second thermocouple is mounted as safety feature at the heating sleeve and shuts off the heating, if the temperature of the heating sleeve reaches its maximum temperature. In the window zone, several channels inside the reactor and the sealing plates can be filled with either hot air for heating or a cooling liquid for creating temperature gradients (Figure 1a shows channels in plates, Figure 1c shows channels in reactor). Two different configurations were tested in our experiments: In the first configuration (heating configuration 1) the window zone was heated with hot air through channels inside the sealing plates (Figure 1a and Figure S1, Supporting Information). Hot air was generated from a gas blower (Leister LE mini sensor kit 800 W) with a flow of 15 L min^{-1} and connected to the plates. The hot air blower should not be operated above 700 °C according to the manual, on a minimum of 15 L min^{-1} flow of air. For inducing lower temperatures, e.g., for condensation, a cooling liquid was dosed through a channel close to the window zone and opposite of the hot air entrance. This configuration was used for the experiments shown in this study. In the second configuration (heating configuration 2), both channels inside the reactor close to the catalyst bed were used. On one side, hot air was flowing to heat the window area. On the opposite side, a cooling liquid was dosed. The latter configuration enables a stronger temperature gradient formation inside the catalyst bed and was applied in our recent study.[7] These two configurations are only two examples, there are other configurations possible due to several channels in the reactor and reactor plates. To monitor the temperature in the window zone,

thermocouples were placed in one–end–closed channels with their tips close to the catalyst bed (Figure S2, Supporting Information). The operational temperature of the reactor design should not exceed 350 °C.

2.2. Installation at Synchrotron Radiation Source

The reactor was installed at the beamline by placement inside a dedicated and self–built holder in between the ion chambers, with the window zone placed at the same height as the X–ray beam (Figure S3, Supporting Information). Furthermore, the holder was located on a movable stage, allowing accurate positioning of the window zone in the X-ray beam and enabling spatially–resolved *operando* XAS measurements. The reactor installed at the beamline P65 at the Deutsches Elektronen-Synchrotron (DESY) is shown in Figure S3, Supporting Information. The reactor was packed in heat insulating tape to reduce heat loss, except for the windows (Figure S1b, Supporting Information). The 10 × 10 mm window area allows tracking changes inside the catalyst bed (size 7.5 × 6 mm) in the window zone with spectroscopy (Figure 1c, inset window zone, marked with pink spots) in spatially–resolved manner. Several positions of the bed can be monitored by using a beam size of 0.3 mm (vertical) × 1.6 mm (horizontal). During the experiments, a 3 × 3 matrix was scanned in order to examine the possible influence of the induced temperature gradients on the catalyst structure.

2.3. Mobile Setup Unit

To enable measurements at high pressure (≥90 bar) and control the different heating and cooling sources, as well as temperature monitoring, a mobile setup unit was planned and built. A schematic diagram of the setup is depicted in **Figure 2**a, and a photograph of the gas dosing unit is shown Figure 2b.

Gases (H_2 and N_2) were dosed via high–pressure mass flow controllers (Bronkhorst), which are operable until 150 bar. For

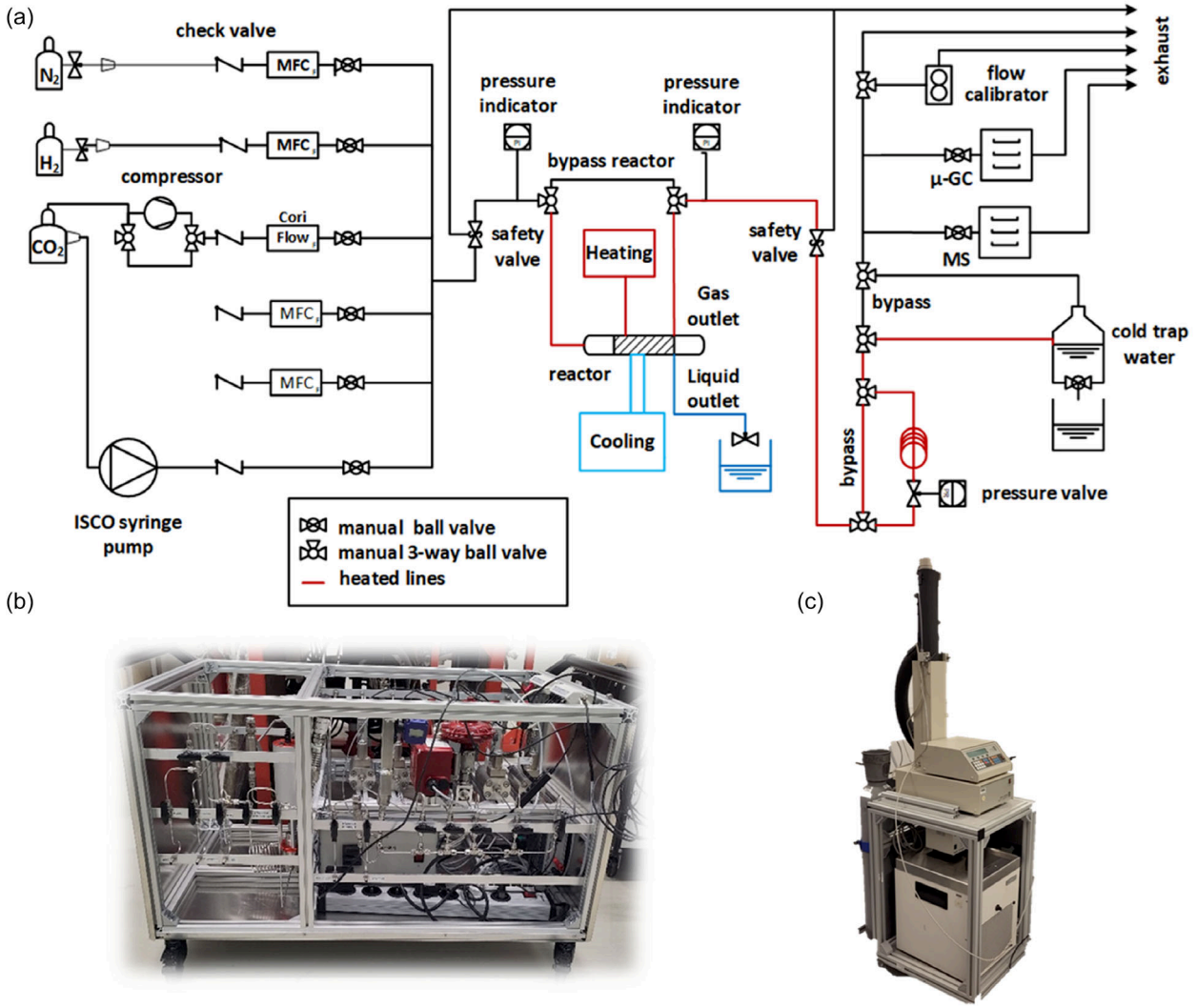

Figure 2. a) Schematic diagram of mobile *operando* setup for the use at synchrotron facilities and operating the additively manufactured reactor. b) Photograph of the gas dosing unit. c) Picture of ISCO pump 260D with installed cooling.

experiments performed at 40 bar, CO_2 was dosed as gas via a mass flow controller (Bronkhorst). For experiments above 54 bar, no direct CO_2 from pressurized gas cylinders can be used as CO_2 is present in liquid form. Therefore, liquid CO_2 was used for experiments at 90 bar and can either be pressurized through a compressor and then fed into a liquid flow controller (CoriFlow, Bronkhorst) or be dosed using a syringe pump (Teledyne ISCO 260D). In the latter case, the cylinder filled with CO_2 and the respective pipes need to be cooled to 0 °C to keep CO_2 in liquid phase (Figure 2c). For the experiments described in this study, CO_2 was dosed *via* mass flow controller at 40 bar. Two additional mass flow controllers are implemented in this setup (one was used for gaseous CO_2), which would, e.g., allow experiments with co-dosed CO. The pressure was controlled using a back–pressure regulator (Swagelok) equipped with an electric actuator (GULEX) for remote control. For safety reasons, overpressure valves were installed, which open at 5 bar above the used operation pressure. For pressure monitoring, two digital pressure indicators were placed before and after the reactor. All lines connected to the reactor were heated to 150 °C using heating lines (HORST). The setup further allowed sampling of the formed liquid products by condensing them after depressurization in a cooling trap. The gas composition was analyzed using a mass spectrometer (Omnistar GSC 320, Pfeiffer Vacuum) and a micro–gas chromatograph (Inficon Fusion Micro–GC, PoraPLOT Q column, 10 m length and 0.25 mm diameter with He carrier gas and a mole sieve column with 5 Å, 0.25 mm diameter, 10 m length and Ar carrier gas).

2.4. Spectra Quality and Validation

The functionality and potential of the *in situ/operando* reactor and setup were tested by examining a $Cu/ZnO/ZrO_2$ catalyst with hard X-rays. The catalyst has a similar composition to industrial catalysts and is highly active in CO_2-based methanol synthesis. More catalyst details can be found in our previous publication.[7] In short, the catalyst was prepared by continuous co-precipitation and has a ratio of Cu:Zn:Zr = 63:29:8 (mol%). First, the spectra quality recorded at room temperature and ambient pressure will be discussed. This is important because, in order to compare the catalyst state after different treatments independently of the conditions applied during the reaction, XAS spectra were recorded at room temperature after each reaction step. The spectra recorded at the Cu K edge after reduction of the $Cu/ZnO/ZrO_2$ catalyst and a Cu foil are shown in **Figure 3**a. The catalyst spectrum matches with the main characteristics of the Cu foil, leading to the conclusion that Cu is in the reduced state. From these spectra the Fourier transformed extended X-ray absorption fine structure (EXAFS) part was extracted shown in Figure 3b. The catalyst structure has the first shell maxima at the same position as the Cu foil, however, at a lower intensity. This indicates that Cu in the catalyst has a higher disorder, which is expected since from other characterization techniques, nanostructured Cu is proposed.[7] To further validate the spectra quality, a first shell fit on the EXAFS part was conducted (Figure 3c and Table S1, Supporting Information). The coordination number is 10.9 which is below the coordination number of 12 present in a bulk Cu structure, confirming the nanostructured nature of the catalyst.

2.5. Temperature Programmed Reduction at Ambient Pressure

The abovementioned $Cu/ZnO/ZrO_2$ catalyst is applied in CO_2-based methanol synthesis. Prior to reaction, the catalyst needs to be activated via reduction at elevated temperatures, in this case with 10% H_2/N_2 to reduce CuO to Cu. Spectra recorded at the Cu K during the reduction (i.e., while dosing reductive gases and at elevated temperatures) are shown in **Figure 4**a. The changes observed in the spectra can be assigned to the reduction of CuO to Cu by comparison with a CuO reference and Cu foil. Furthermore, with linear combination analysis (LCA), the concentration profile during the reduction was investigated and is displayed in Figure 4b. The main reduction starts when the setpoint temperature of 220 °C is reached. The spectra recorded at the Zn K edge during activation and their interpretation can be found in the (Section 2, Figure S5, Supporting Information). The initially present ZnO was not reduced to Zn as in the case for CuO, nevertheless, small changes in the spectra were recorded. By comparison with literature, we propose the possible formation of oxygen vacancies in ZnO (see further details in Section 2, Supporting Information).

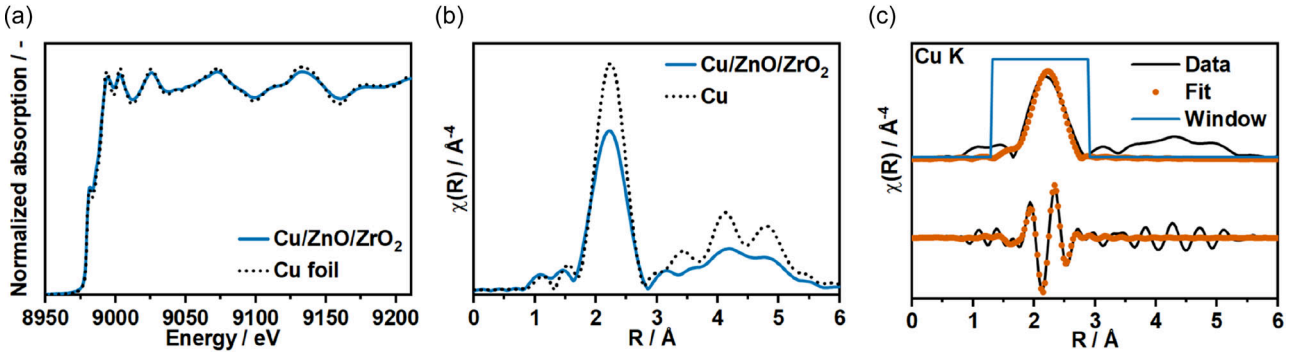

Figure 3. a) X-ray absorption near edge structure (XANES) recorded at Cu K edge of a reduced $Cu/ZnO/ZrO_2$ catalyst (blue) and Cu foil (dotted black), b) the extracted EXAFS, and c) a first shell fit of the catalyst with more details in the Supporting Information (Table S1).

Research Article
doi.org/10.1002/cmtd.202500105
Chemistry Europe
European Chemical Societies Publishing

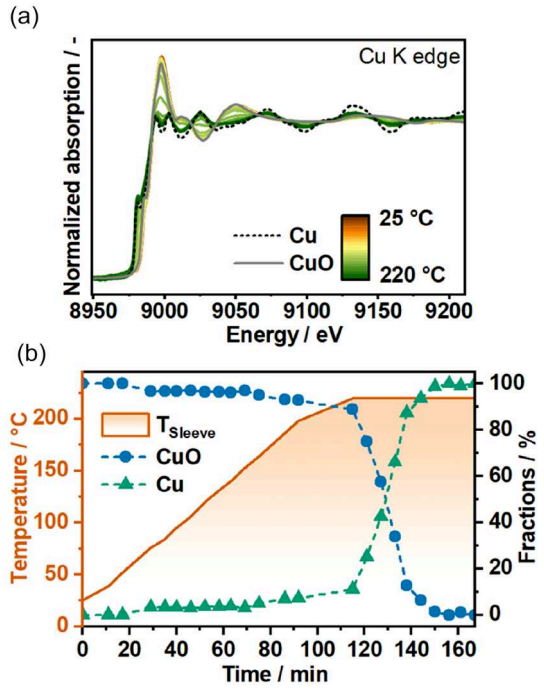

Figure 4. a) XANES recorded at the Cu K edge during reduction (10%H_2/N_2, 220 °C with 2 K min^{-1}) of the Cu/ZnO/ZrO_2 catalyst and Cu and CuO references b) temperature and concentration profile, concentrations obtained by LCA.

3. *Operando* XAS of Cu/ZnO/ZrO_2 during CO_2 Hydrogenation and Condensation

After catalyst activation, CO_2 hydrogenation to methanol was carried out (reac1) at 40 bar and 220 °C. Under these conditions, a CO_2 conversion (X_{CO2}) of ≈21% was achieved with a 70% MeOH selectivity (S_{MeOH}) during 1.5 h time on stream (Figure S6, Supporting Information). Throughout the complete experiment, no significant changes at the Cu K edge during the reaction states were observed (see Figure S7, Supporting Information). Therefore, only data recorded at Zn K edge is discussed in the following. During reaction, a shoulder emerged at 9664 eV (see **Figure 5**a) which indicates restructuring during reaction conditions. To further exploit the dual catalyst bed configuration with different temperature zones, the catalyst was investigated during enforced condensation of the products. After the initial reaction, the temperature in the window zone was decreased by introducing a cooling liquid with varied temperatures (reac2 + reac3) and additionally decreasing the temperature of the gas blower. In the last step, the temperature in the window zone was decreased to 40 °C with the aim to induce condensation (final). In contrast to Cu, ZnO underwent strong restructuring during the whole experiment (Figure 5a, recorded at the middle position (Pos. 5)). By comparing the reduced state (black) with the states after reac1–reac3 (gray), an emerging shoulder at 9664 eV could be observed. The final state exhibited a strong increase in the white line, and the first maximum was shifted to lower energy. In earlier investigations of the catalyst,[7] we identified three different ZnO_x species using multivariate curve resolution least square analysis (MCR-ALS) during CO_2-to-methanol synthesis shown in Figure 5b: A defective wurtzite-type ZnO structure, which was present after the activation (green spectra), a dispersed dimeric ZnO_x species (pink spectra), and a $ZnCO_3$ structure (blue spectra). The dispersed dimeric ZnO_x species was observed during reaction with high CO_2 conversion, resulting in large methanol and water concentrations. We observed $ZnCO_3$ formation upon condensation in the catalyst bed. These spectra were used as references for LCA to quantify the different reaction states in the herein reported study (Figure 5c). After the first reaction (reac1), the main fraction stayed in the initial w-ZnO state (96%), and 4% of disordered dimeric ZnO_x was detected. After introducing the cooling liquid (reac2 + reac3), the dimeric ZnO_x increased to 14% and w-ZnO decreased to 86%. In the final state, the condensation led to formation of 80% $ZnCO_3$ while 20% dimeric ZnO_x remained. The in situ formation of $ZnCO_3$ under condensation conditions may indicate restructuring pathways relevant to catalyst deactivation, particularly at the end of industrial catalyst beds where water and methanol could condense. This structural evolution of Zn under condensation is especially relevant for CO_2 hydrogenation plants, where liquid byproduct accumulation at the catalyst bed outlet is known to accelerate deactivation and complicate long-term stability. Capturing this transition *operando*, rather than relying on *ex situ*

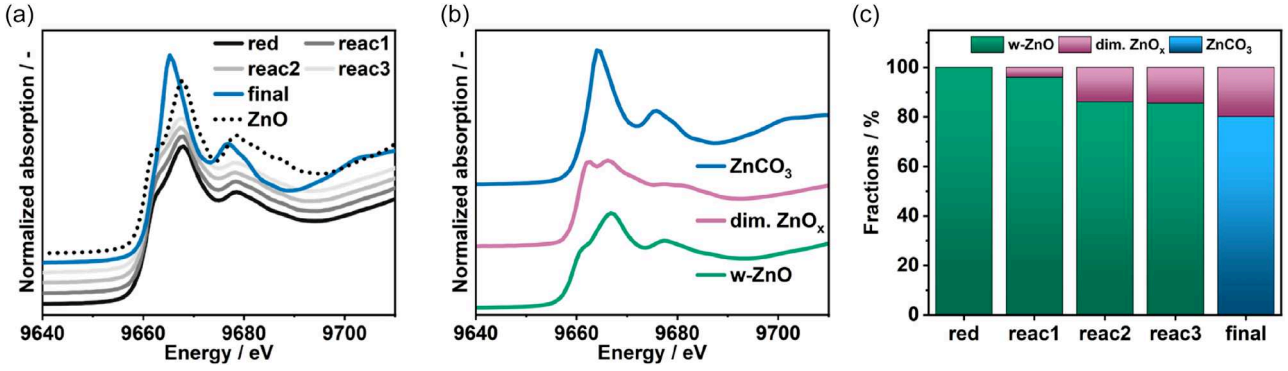

Figure 5. a) XANES recorded at the Zn K edge after reduction (red), various reaction steps (reac1–reac3, final) and a ZnO reference, b) three components resulted from MCR-ALS analysis in a previous study,[7] and c) fractions of the three components (ZnO, dimeric ZnO_x, $ZnCO_3$) obtained by LCA for the different reaction steps.

analysis, highlights the importance of studying structural dynamics under realistic process conditions.

3.1. Spatially-Resolved Measurements

As shown in the inset in Figure 1c, an additional feature of the reactor is the possibility to conduct spatially-resolved measurements. During the experiment, a 3 × 3 matrix was scanned at different reaction steps at room temperature (Figure S4a, Supporting Information). After reduction and the reaction steps 1–3, no differences between the 9 recorded positions were observed (see Figure S8, Supporting Information). However, during the final state, variations between the different positions were observed and are shown in **Figure 6**a–c (each figure shows spectra recorded in one column). By comparing the spectra at different positions, a gradient in vertical direction could be revealed (e.g., Figure 6a for Pos. 1,4,7). The spectra in the top row (Pos. 1–3) have a higher white line intensity which is decreasing in flow direction (4–9). The changes were further quantified with LCA analysis using the three references shown in Figure 5b. The top row (Pos. 1–3) exhibited 100% $ZnCO_3$ (Figure 6d). In the middle row, the $ZnCO_3$ fraction decreased to 91% for Pos. 4 and 80% for Pos. 6, with dimeric ZnO_x being the other species. In the last row, the amount of $ZnCO_3$ stayed similar for Pos. 8 and 9, while for Pos. 7 an even lower amount of $ZnCO_3$ (72%) was found. The spectra were not recorded in the order of the position name (1–9), but in a manner to only move one motor at the same time. Therefore, we can exclude that the changes observed are a time effect. One explanation for the vertical gradient could be that the condensed products enter the top of the catalyst bed first. This could explain the more severe changes at Pos. 1–3.

4. Conclusion

The application of AM using laser-based metal powder bed fusion for designing the catalytic and spectroscopic reactor has been presented in this work which allowed to integrate the following essential features: 1) An X–ray transparent window zone for monitoring the catalyst structure during reaction, also in a spatially-resolved manner and 2) two consecutive catalyst beds with independent controllable heating. The dual catalyst bed configuration allows to simulate different positions of a fixed-bed reactor depending on the amount of catalyst used in the upper part. The reactor complements the recently developed concept "Iso-potential *operando* spectroscopy" where the local gas environment in a spatial-profile reactor at a certain position gets transferred to a spectroscopic reactor, separating catalytic reactor, and spectroscopic cell.[10,55] In contrast to previous *operando* setups, this design enables *operando* investigations of catalysts at medium and high conversion levels and under condensation conditions; scenarios that have remained experimentally inaccessible despite their industrial relevance. For the use at synchrotron facilities, a mobile setup unit was constructed with a compact design and remote–control capabilities for all critical reaction

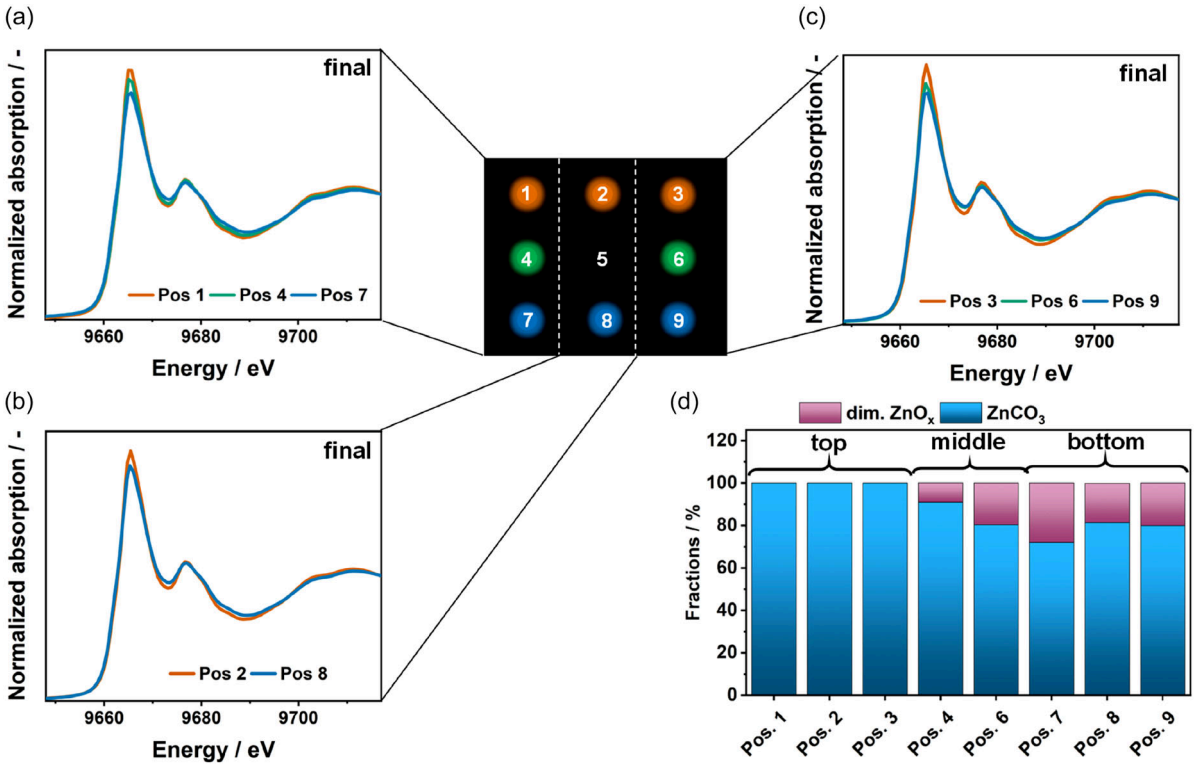

Figure 6. XANES recorded at 9 positions in 3 × 3 matrix at the final state at a) Pos. 1 + 4 + 7, b) Pos. 2 + 8 (Pos. 5 was unsuitable for data treatment), c) Pos. 3 + 6 + 9, and d) LCA results of 8 different positions recorded during final state obtained with MCR-ALS components used above.

parameters (temperature, gas flow, and pressure). The reactor functionality was probed by *operando* XAS investigations in CO_2-based methanol synthesis. The new setup and cell allowed to study the structure of a Cu/ZnO/ZrO_2 catalyst under high conversion and enforced condensation conditions, mimicking catalysts under high stress, which is typical for the end of a catalyst bed if liquid by–products like water are formed. Restructuring of ZnO could be observed with the formation of dispersed ZnO_x species and $ZnCO_3$ during condensation. These findings reinforce the importance of studying catalyst deactivation mechanisms under true end-of-bed conditions, where liquid product formation and thermal gradients may induce irreversible structural changes. Furthermore, the large window area of 10×10 mm enabled spatially-resolved measurements with the opportunity to measure at 9 different positions. With this feature, gradients along the catalyst bed can be tracked, as shown for the final state, which exhibited a vertical gradient of the $ZnCO_3$ concentration.

AM is a powerful tool and holds extensive potential, especially in spectroscopy application where often small channels and structures are necessary. In the future, metal-based AM should be further utilized for designing catalytic reactors and spectroscopic cells, taking advantage of its customization capabilities. This allows for more spectroscopic features and the combination of complementary techniques. For example, the current design can be slightly modified for *operando* X-ray diffraction studies. Additionally, replacing the Be windows with materials like sapphire would enable visual tracking of condensation either by a camera or the catalyst might be investigated by UV–vis/IR spectroscopy depending on the transmission properties of the material. The dual catalyst bed concept with condensation zone can further be applied to various other reactions, such as methanation, Fischer–Tropsch reaction, and ammonia synthesis. However, before adapting the concept to another reaction or conditions, careful evaluation of the safety aspects in relation to materials compatibility needs to be considered. Altogether, the integration of AM with *operando* spectroscopy marks a decisive step toward more realistic and flexible catalyst characterization platforms.

5. Experimental Section

The used Cu/ZnO/ZrO_2 (CZZ) catalyst in this study is described in more detail in the following references with *ex situ* characterization.[7,56] The *operando* experiment was conducted at DESY, Hamburg, at beamline P65.[57] The first ion chamber was filled with 10% Ar in N_2 at 1020 mbar, the second one with 25% Ar in N_2 at 1020 mbar, and third with 100% Kr. The beam size was 0.3 mm (vertical) $\times$ 1.6 mm (horizontal). The spectra were measured in transmission mode, with the reactor positioned between ionization chambers 1 and 2, and a Cu reference foil placed between ion chambers 2 and 3. During the experiment, both K edges were recorded in a single scan (8.8–10.6 keV), using the Cu foil for alignment. The CZZ catalyst was mixed with SiO_2 in a 1:9 ratio, pressed to achieve a sieve fraction of 100–200 µm, and 24 mg of this mixture was placed in the reactor window zone. Approximately 1 g of undiluted catalyst (sieve fraction 100–200 µm) was filled in the upper part of the reactor. The reactor was then mounted on a holder, which could be positioned on the sample alignment stage between the ionization chambers. To manufacture the high-pressure reactor system additively, the metal laser powder bed fusion method, commonly known as "3D printing," was utilized on an EOS M290 single laser machine. The process involved melting nickel-based superalloy powder (alloy 625, UNS N06625; W. Nr. 2.4856) with particle sizes ranging from 10 to 45 microns using an infrared laser with a maximum power of 400 W. Different laser modes were applied to create both solid and porous metal sections. The tightness of the completed assembly, including the AM-made parts, the sealing system, and the fittings, was verified using a Helium leak test, achieving a rate of $24{\cdot}10^{-10}$ mbar L s^{-1}. The pressure resistance was confirmed through a water pressure test, successfully withstanding an internal pressure of 350 bar without deformation. Prior to use at the synchrotron, the assembly's tightness was further tested with 150 bar nitrogen, showing no changes over a period of two hours. For this experiment, heat configuration 1 (Figure S1, Supporting Information) was used. The overall experimental procedure is shown in Figure S4, Supporting Information. Prior to reaction, the catalyst was activated via temperature programmed reduction at 220 °C (1 h, ramp 2 °C min^{-1}) in 10% H_2 in N_2. After catalyst activation, CO_2 hydrogenation to methanol was carried out using a reaction mixture of 85% H_2:CO_2 = 3.1 in N_2 at 220 °C and 40 bar. Gaseous CO_2 was supplied via a Bronkhorst mass flow controller during this experiment. For the following reaction, different temperatures of the cooling liquid were used to achieve temperature variations in the window zone. The temperature of the cooling liquid was decreased stepwise with temperatures of 25, 10, and 0 °C during reac2, while −20 °C was used for reac3. In the final reaction step (reac4), the temperature of the cooling liquid was set to 25 °C. Additionally, the temperature of the gas blower was first reduced to 200 °C, before final cooling to 25 °C (final state). During the experiment, the temperature of the upper part (T_{sleeve}), of the outlet of the gas blower (T_{GB}), and inside the window zone (T_1–T_3) (see Figure S2, Supporting Information for placement of the thermocouples) were recorded and are displayed in Figure S4b, Supporting Information. During transient conditions, XAS was recorded at one position (Pos 5, see Figure 1c). After several steps, the reactor was cooled to room temperature for EXAFS scans, and 9 positions in the catalyst bed were measured (3 x 3 point maps through the rectangular window, see Figure 1c). The positions were scanned in the following order: 7, 1, 2, 3, 6, 9, 8, 5, 4. All spectra were energy corrected and normalized using the Fastosh software package (version 1.0.7–pre-release).[58] Then, LCA was applied, using the same software.

Supporting Information

Additional results can be found in the Supporting Information of this article. The authors have cited additional references within the Supporting Information.[59–61]

Acknowledgements

The authors extend their gratitude to Jan Pesek (ITCP, KIT), Siegbert Johnson (IKFT, KIT), and the KIT workshop for support during the construction and installation of the applied experimental setup. The authors acknowledge Dr. Marc-André Serrer (ITCP, KIT), Uliana Söllner (Siemens), Dr. Robert Otto (Siemens), Dr. Denis Krompass (Siemens), and Dr. Yves Küsters (Siemens) for valuable feedback during the development of the spectroscopic cell. The authors thank Diana Deutsch, Thomas Zevaco,

Gabriela Rodrigues Niquini, Dr. Karla Herrera-Delgado, Dr. Lucas Warmuth, and Dr. Stephan Pitter (all IKFT, KIT) for their efforts in catalyst preparation, ex situ characterization, and engaging discussions on reactor design and Cu-Zn-based catalyst systems. The authors are grateful to Dr. Anna Zimina, Dr. Danielle Santos Goncalves, and Markus Makowiak (all ITCP, KIT) for their assistance in beamtime preparation. For insightful discussions on Cu-Zn based catalyst systems and their characterization, the authors thank Dr. Arik Beck. Additionally, the authors acknowledge the DESY, a member of the Helmholtz Association HGF, for the providing experimental facilities for beamtime. Parts of this research were conducted at PETRA III on beamline P65 under proposal number I-20230260, and the authors thank Dr. Edmund Welter, Regina Biller, and Marcel Görlitz for their support. For beamtime support and discussion on data evaluation, the authors thank Dr. Dmitry Doronkin (IKFT, KIT). The authors gratefully acknowledge the funding of the BMWE Verbundvorhaben 3D-PROCESS (reference numbers 03EN2065B and 03EN2065D) by the German Federal Ministry for Economic Affairs and Energy.

Open Access funding enabled and organized by Projekt DEAL.

Conflict of Interest

The authors declare no conflict of interest.

Data Availability Statement

The data that support the findings of this study are available in the supplementary material of this article.

Keywords: additive manufacturing · CO_2-based methanol · heterogeneous catalysis · operando · X-ray absorption spectroscopy

[1] K. F. Kalz, R. Kraehnert, M. Dvoyashkin, R. Dittmeyer, R. Gläser, U. Krewer, K. Reuter, J.-D. Grunwaldt, *ChemCatChem* **2017**, *9*, 17.
[2] A. T. Bell, *Science* **2003**, *299*, 1688.
[3] M. A. Newton, *Chem. Soc. Rev.* **2008**, *37*, 2644.
[4] R. Schlögl, *Angew. Chem. Int. Ed.* **2015**, *54*, 3465.
[5] B. M. Weckhuysen, *Natl. Sci. Rev.* **2015**, *2*, 147.
[6] B. B. Sarma, J.-D. Grunwaldt, *CHIMIA* **2024**, *78*, 288.
[7] M. L. Schulte, V. Truttmann, D. E. Doronkin, L. Baumgarten, A. Nicolai, D. A. M. Beltran, F. J. Summ, C. Kiener, L. Warmuth, S. Pitter, E. Saraçi, J.-D. Grunwaldt, *Angew. Chem. Int. Ed.* **2025**, *64*, e202423281.
[8] J.-D. Grunwaldt, B. S. Clausen, *Top. Catal.* **2002**, *18*, 37.
[9] S. R. Bare, T. Ressler, in *Advances in Catalysis*, vol. *52*, Academic Press, San Diego, **2009**, 339–465.
[10] S. Sichert, S.-F. Stahl, O. Korup, R. Horn, *ACS Catal.* **2024**, *14*, 8676.
[11] A. Beck, V. Paunović, J. A. van Bokhoven, *Nat. Catal.* **2023**, *6*, 873.
[12] S. Chen, J. Jelic, D. Rein, S. Najafishirtari, F.-P. Schmidt, F. Girgsdies, L. Kang, A. Wandzilak, A. Rabe, D. E. Doronkin, J. Wang, K. F. Ortega, S. Debeer, J.-D. Grunwaldt, R. Schlögl, T. Lunkenbein, F. Studt, M. Behrens, *Nat. Commun.* **2024**, *15*, 871.
[13] A. Bansode, A. Urakawa, *J. Catal.* **2014**, *309*, 66.
[14] J. Topp-Jørgensen, in *Surf. Sci. Catal.* (Eds: D. M. Bibby, C. D. Chang, R. F. Howe, S. Yurchak), vol. *36*, Elsevier **1988**, pp. 293–305.
[15] D. E. Doronkin, H. Lichtenberg, J.-D. Grunwaldt, *in XAFS Techniques for Catalysts, Nanomaterials, and Surfaces*, Springer International Publishing **2017**, pp. 75–89.
[16] D. E. Doronkin, J.-D. Grunwaldt, in *Chemical Energy storage* (Ed: R. Schlögl), 2 ed., Walter de Gruyter, Berlin/Boston **2013**, pp. 369–392.
[17] J.-D. Grunwaldt, R. Wandeler, A. Baiker, *Catal. Rev. Sci. Eng.* **2003**, *45*, 1.
[18] G. H. Via, J. H. Sinfelt, F. W. Lytle, *J. Chem. Phys.* **1979**, *71*, 690.
[19] L. Pandit, M. A. Serrer, E. Saraçi, A. Boubnov, J.-D. Grunwaldt, *Chem. Methods* **2022**, *2*, e202100078.
[20] J.-D. Grunwaldt, M. Caravati, S. Hannemann, A. Baiker, *Phys. Chem. Chem. Phys.* **2004**, *6*, 3037.
[21] B. S. Clausen, G. Steffensen, B. Fabius, J. Villadsen, R. Feidenhans'l, H. Topsøe, *J. Catal.* **1991**, *132*, 524.
[22] A. Tsoukalou, P. M. Abdala, D. Stoian, X. Huang, M.-G. Willinger, A. Fedorov, C. R. Müller, *J. Am. Chem. Soc.* **2019**, *141*, 13497.
[23] M. Zabilskiy, V. L. Sushkevich, D. Palagin, M. A. Newton, F. Krumeich, J. A. van Bokhoven, *Nat. Commun.* **2020**, *11*, 2409.
[24] A. Beck, M. Zabilskiy, M. A. Newton, O. Safonova, M. G. Willinger, J. A. van Bokhoven, *Nat. Catal.* **2021**, *4*, 488.
[25] M. T. Nikolajsen, J.-C. Grivel, A. Gaur, L. P. Hansen, L. Baumgarten, N. C. Schjødt, U. V. Mentzel, J.-D. Grunwaldt, J. Sehested, J. M. Christensen, M. Høj, *J. Catal.* **2024**, *431*, 115389.
[26] T. P. Araújo, G. Giannakakis, J. Morales-Vidal, M. Agrachev, Z. Ruiz-Bernal, P. Preikschas, T. Zou, F. Krumeich, P. O. Willi, W. J. Stark, R. N. Grass, G. Jeschke, S. Mitchell, N. López, J. Pérez-Ramírez, *Nat. Commun.* **2024**, *15*, 3101.
[27] M. Yang, J. Yu, A. Zimina, B. B. Sarma, L. Pandit, J.-D. Grunwaldt, L. Zhang, H. Xu, J. Sun, *Angew. Chem. Int. Ed.* **2023**, *62*, e202216803.
[28] P. Ticali, D. Salusso, R. Ahmad, C. Ahoba-Sam, A. Ramirez, G. Shterk, K. A. Lomachenko, E. Borfecchia, S. Morandi, L. Cavallo, J. Gascon, S. Bordiga, U. Olsbye, *Catal. Sci. Technol.* **2021**, *11*, 1249.
[29] O. Martin, C. Mondelli, A. Cervellino, D. Ferri, D. Curulla-Ferré, J. Pérez-Ramírez, *Angew. Chem. Int. Ed.* **2016**, *55*, 11031.
[30] A. Bansode, G. Guilera, V. Cuartero, L. Simonelli, M. Avila, A. Urakawa, *Rev. Sci. Instrum.* **2014**, *85*, 084105.
[31] S. R. Bare, N. Yang, S. D. Kelly, G. E. Mickelson, F. S. Modica, *Catal. Today* **2007**, *126*, 18.
[32] N. J. Divins, D. Kordus, J. Timoshenko, I. Sinev, I. Zegkinoglou, A. Bergmann, S. W. Chee, S. Widrinna, O. Karslıoğlu, H. Mistry, M. L. Luna, J. Q. Zhong, A. S. Hoffman, A. Boubnov, J. A. Boscoboinik, M. Heggen, R. E. Dunin-Borkowski, S. R. Bare, B. R. Cuenya, *Nat. Commun.* **2021**, *12*, 1435.
[33] B. S. Clausen, H. Topsøe, *Catal. Today* **1991**, *9*, 189.
[34] A. Rochet, V. Moizan, C. Pichon, F. Diehl, A. Berliet, V. Briois, *Catal. Today* **2011**, *171*, 186.
[35] A. Nassereddine, A. Prat, S. Ould-Chikh, E. Lahera, O. Proux, W. Delnet, A. Costes, I. Maurin, I. Kieffer, S. Min, M. Rovezzi, D. Testemale, J. L. C. Olmo, J. Gascon, J.-L. Hazemann, A. A. Tapia, *Rev. Sci. Instrum.* **2024**, 95.
[36] I. Gibson, D. W. Rosen, B. Stucker, M. Khorasani, D. Rosen, B. Stucker, M. Khorasani, *in Additive Manufacturing Technologies*, 3rd ed., Springer Nature Switzerland AG, Cham **2021**, pp. 125–170.
[37] O. H. Laguna, P. F. Lietor, F. J. I. Godino, F. A. Corpas-Iglesias, *Mater. Des.* **2021**, *208*, 109927.
[38] C. Parra-Cabrera, C. Achille, S. Kuhn, R. Ameloot, *Chem. Soc. Rev.* **2018**, *47*, 209.
[39] E. Kozyr, S. Marti-Sanchez, A. Skorynina, J. Arbiol, C. Escudero, L. Mino, A. Bugaev, *J. Synchrotron Rad.* **2024**, *31*, 1071.
[40] F. Mehdipour, T. Delrieux, F. Maurer, J.-D. Grunwaldt, C. Klahn, R. Dittmeyer, *Catal. Commun.* **2024**, *187*, 106873.
[41] C. Y. Chaparro-Garnica, P. Jordá-Faus, E. Bailón-García, R. Ocampo-Pérez, C. G. Aguilar-Madera, A. Davó-Quiñonero, D. Lozano-Castelló, A. Bueno-López, *ACS Appl. Mater. Interfaces* **2020**, *12*, 54573.
[42] R. Dittmeyer, C. Kiener, C. Klahn, V. Schulze, *Chem. Ing. Tech.* **2022**, *94*, 919.
[43] A. Bernard, C. Klahn, M. Biedermann, *in Springer Handbook of Additive Manufacturing* (Ed:E. Pei), Springer International Publishing, Cham **2023**, pp. 907–922.
[44] M. Fuchs, J. Bodemer, S. Kabelac, *Int. J. Heat Mass Transfer* **2024**, *218*, 124774.

[45] G. E. Achkar, C. Septet, O. L. Metayer, J.-M. Hugo, *Int. J. Heat Mass Transfer* **2022**, *199*, 123465.
[46] E. Hansjosten, A. Wenka, A. Hensel, W. Benzinger, M. Klumpp, R. Dittmeyer, *Chem. Eng. Process.* **2018**, *130*, 119.
[47] C. Kiener, S. Boschert, Y. Küsters, A. Nicolai, R. Otto, *Chem. Ing. Tech.* **2022**, *94*, 1040.
[48] C. Kiener (Siemens AG), EP-4438206A1 **2024**.
[49] C. Kiener, R. Otto, A. Nicolai (Siemens AG), EP-4282505A1 **2023**.
[50] C. Kiener (Siemens AG), EP-3736519A1 **2020**.
[51] C. Kiener (Siemens AG), WO-2020020689A1 **2020**.
[52] C. Kiener (Siemens AG), EP-4548990A1 **2025**.
[53] P. Schwiderowski, H. Ruland, M. Muhler, *Curr. Opin. Green Sustain. Chem.* **2022**, *38*, 100688.
[54] F. Grinschek, B. Ladewig, A. N. Munoz, C. Klahn, R. Dittmeyer, *Chem. Ing. Tech.* **2022**, *94*, 931.
[55] R. Horn (Reacnostics GmbH) EP-4049022B1 **2024**.
[56] L. Warmuth, M. Steurer, D. Schild, A. Zimina, J.-D. Grunwaldt, S. Pitter, *ACS Appl. Mater. Interfaces* **2024**, *16*, 8813.
[57] E. Welter, R. Chernikov, M. Herrmann, R. Nemausat, *AIP Conf. Proc.* **2019**, *2054*, 040002.
[58] G. Landrot, E. Fonda, *J. Synchrotron Rad.* **2025**, *32*, 1085.

Manuscript received: July 31, 2025
Revised manuscript received: October 19, 2025
Version of record online: